click for updates

CrystEngComm

Accepted Manuscript

Volume 18 | Number 1 | 7 January 2016 | Pages 1–184

CrystEngComm

www.rsc.org/crystengcomm

ROYAL SOCIETY OF CHEMISTRY

HIGHLIGHT
Tiddo J. Mooibroek, Antonio Frontera et al
Towards design strategies for anion–π interactions in crystal engineering

175 YEARS

ROYAL SOCIETY OF CHEMISTRY

rsc.li/crystengcomm

On the mechanisms of hydrogen induced blistering
in RF sputtered amorphous Ge

M. Serényi[1], C. Frigeri[2,*], A. Csik[3], N. Q. Khánh[1], A. Németh[4], Z. Zolnai[1]

[1] Institute of Technical Physics and Materials Science, Research Centre for Natural Sciences, Hungarian Academy of Sciences, P.O. Box 49, H-1525 Budapest, Hungary

[2] CNR-IMEM Institute, Parco Area delle Scienze 37/A, 43100 Parma, Italy

[3] Institute for Nuclear Research, Hungarian Academy of Sciences, P.O. Box 51, H-4001 Debrecen, Hungary

[4] Institute for Particle and Nuclear Physics, Wigner Research Centre for Physics, Hungarian Academy of Sciences, P.O. Box 49, H-1525 Budapest, Hungary

*Corresponding Author: frigeri@imem.cnr.it, Tel: +39 0521 269235

Abstract

Hydrogenated amorphous germanium, *a*-Ge:H, is a material of interest for optoelectronic applications such as solar cells and radiation detectors because of the material's potential to extend the wavelength sensitivity of hydrogenated amorphous silicon. For such applications the best structural quality is required. Here we investigate the mechanisms of blister formation in a-Ge:H films obtained by RF (radio frequency) sputtering when submitted to annealing. By a Fourier Transform IR spectroscopy study of the Ge-H stretching vibrations it is found that annealing increases the density of GeH_2 dihydrides residing on the internal surfaces of nanovoids which increase their size because of that. The thermal energy supplied by annealing also favours the break of the Ge-H bonds with consequent release inside the cavities of atomic H which then reacts to produce molecular H_2. The expansion of the H_2 gas makes the nanovoids to enhance their volume

1

up to the formation of surface blisters. The presence of H_2 in the blisters is confirmed by the activation energy for the onset of blistering as measured by Arrhenius plots. The reduced H content observed by Elastic Recoil Detection Analysis and Secondary Neutral Mass Spectrometry in the annealed samples where blister bursting took place further supports the hypothesis of H_2 filling the blisters before they explode.

Keywords : Blisters; Hydrogen; Amorphous Ge; Annealing; Sputtering; Solar cells

1 . Introduction

The most typical applications of hydrogenated amorphous Ge (a-Ge:H) concern solar cells and infrared optics beside others like detectors for x- or γ- ray imaging, fiber-optic systems and transistors [1-3]. As to solar cells, a-Ge:H is used as the bottom low bandgap (1.1 eV) absorber in tandem solar cells with a-Si as the top high bandgap (1.7 eV) cell so as to harvest a larger portion of the solar spectrum. a-Ge:H is promising to be a better material as absorber of the longer wavelengths with respect to alternatives like microcrystalline Si (μc-Si:H), microcrystalline SiGe (μc-SiGe:H) and a-SiGe:H alloys [1]. In fact, the electronic properties of the latter two alloys strongly degrade with increasing Ge content (which is necessary to reduce the bandgap) while the μc-Si:H must be grown much thicker than a-Ge:H to get comparable efficiency of the tandem cell with consequent increase of the production costs [1]. Also for infrared sensors, like un-cooled microbolometers, a-Ge:H is a valid replacement of a-Si:H. It has, in fact, a four orders of magnitude higher electrical conductivity, relatively large temperature coefficient of resistance (TCR) and activation energy, which regulates the exponential temperature dependence of the conductivity [2]. All this makes a-Ge:H more suitable for IR detection with respect to a-Si:H [2].

Heat treatments are often applied during deposition of a-Ge:H, e.g. by plasma-enhanced chemical vapour deposition (PECVD) which is carried out either at 160 °C [1] or 200 °C [2]. As regards solar cells, after deposition processing also requires annealing at temperatures of 160 °C and 130 °C (for 15 h) [1]. Furthermore, annealing at 100-150 °C is also used to destroy the unwanted defect states created in a-Si:H upon exposure to the sunlight (Staebler-Wronski effect [4]) of the photovoltaic device [5, 6]. Although a-Ge:H does not seem to exhibit noticeable Staebler-Wronski effect [7, 8], it necessarily undergoes the same annealing treatment as a-Si:H when it is part of a tandem cell.

A wealth of works have reported on the degradation of the surface by formation of blisters and craters owing to heat treatments in crystalline Si and Ge hydrogenated by H implantation (see e. g. Refs. 9-12) or other H-implanted systems [13]. However, although several papers suggested that microvoids embedded in the a-Si:H could give rise to blisters when a thermal treatment is applied, only a few of them reported on the blister existence in a-Si:H for which hydrogenation was obtained by methods other than implantation [14-19].

Even much less literature exists about blisters/craters in the case of not-implanted hydrogenated a-Ge [20, 21].

In previous studies of our group on a-Si:H layers submitted to annealing it was found that the cause of the structural degradation of the layers in the shape of blisters and craters was the change of the hydrogen bonding configuration [17-20]. In this paper we investigate whether this also occurs in a-Ge:H by submitting as-deposited films with different H content to annealing. For the applications cited earlier a-Ge:H is typically deposited on Si substrates. In preliminary investigations of our own on annealed a-Ge:H/Si samples we had evidence that Fourier transform infrared (FTIR) spectroscopy also detected vibrational modes related to Si-H bonds created in the Si substrate very likely because of H diffusion. One FTIR band of the stretching mode of the Si-H bonds exactly overlaps one of the Ge-H peaks which made troublesome and uncertain the exact evaluation of the latter ones. Since an important part of our work was to carefully study the type and density of the bonds of H to Ge we therefore avoided the use of clean Si substrates. The avoid direct contact between Ge and Si substrate the latter was not cleaned (deoxidized). On the contrary, it was covered with an SiO_x layer. This was achieved by exposing the Si to the laboratory atmosphere for 1 month in order to let the native oxide to grow thicker and thicker. However, also this approach was discarded for two reasons. The a-Ge:H on SiO_x/Si layers exhibited the same features, though to a smaller extent, as the a-Ge:H on Si. Additionally, when SiO_x is used degassing of H_2O and H_2, catalyzed by the O bridging the Si atoms in SiO_x, may occur with formation of morphological bubbles as reported by Valladares et al. [21]. We have thus chosen ZnSe as substrate as it is not expected to have the mentioned inconveniences and is transparent to the IR radiation.

Hereafter we use the notation Ge-H to represent germanium-hydrogen bonds in any GeH_n groupings while GeH and GeH_2 are reserved to the specific single and double groupings, respectively.

2 . Experimental

The hydrogenated a-Ge films were deposited on polished (100) ZnSe wafers in a Leybold Z400 radio frequency (RF) sputtering apparatus from a high purity crystalline Ge target.

The basic pressure in the chamber was $5 \cdot 10^{-5}$ Pa evacuated by a turbo molecular pump. The target was coupled to the RF generator operating at 13.56 MHz. The film thickness was 530 nm as measured with a Tencor AlphaStep 500 instrument. Sputtering has been performed under a mixture of high purity argon and hydrogen gases with an applied wall potential of 1500 V dc yielding a plasma pressure of $2.5_x 10^{-2}$ mbar. The amount of hydrogen to be incorporated into the layers was varied by flowing it continuously into the sputtering chamber at three different partial pressures, i.e. 0.2%, 0.6% and 0.9% of the $2.5_x 10^{-2}$ mbar plasma pressure. Henceforward the H partial pressures will be simply identified as H= 0.2, 0.6 and 0.9, respectively. The effective H concentration in the as-deposited films turned out to be 10.8, 18 and 21 at%, respectively, as measured by ERDA (Elastic Recoil Detection Analysis) and shown in Fig. 1. Both hydrogenated and not-hydrogenated films were submitted to annealing at 135°C for 40 and 120 minutes in high purity (99.999%) argon. The as-deposited and annealed samples were investigated by ERDA, Fourier transform infrared (FTIR) spectroscopy, Secondary Neutral Mass Spectrometry (SNMS), stylus profilometry and Scanning Electron Microscopy (SEM).

The ERDA measurements were carried out with 1.6 MeV ^{4}He$^+$ analysing ion beam at the 5 MeV Van de Graaff accelerator of the Wigner Research Centre for Physics in Budapest on 40 nm thick a-Ge:H layers grown on Si under the same H partial pressures and overall sputtering conditions as applied for the 530 nm thick films. The recoiled H signal was collected in IBM geometry by an ORTEC surface barrier Si detector placed at 20° detecting angle with respect to the ion beam, with the sample tilted by 80° with respect to the beam. The forward scattered He ions were stopped by putting a 6 μm thick Mylar foil in front of the detector to get rid of the background. Further details can be found in Ref. [22]. In addition to ERDA, Rutherford Backscattering Spectrometry (RBS) spectra were also collected in order to calibrate ERDA for the H content by using a Kapton foil with high H content and nominal atomic composition of $C_{22}H_{10}N_2O_5$. Good agreement was found between ERDA and RBS by simulating their spectra with the RBX code [23]. As it was shown, combined ion beam analytical techniques are powerful in the quantitative characterization of multi-component thin layer structures [24].

FTIR spectroscopy was employed to study the type and evolution of the Ge-H bonds by means of a Bruker Tensor 37 spectrometer with 2 cm^{-1} resolution. The spectra were

CrystEngComm Accepted Manuscript

taken in the 400-4000 cm^{-1} range with a Ge/KBr beam splitter while the baseline was corrected by an adjusted polynomial function. The integrated intensity I of an FTIR vibrational mode scales with the concentration N_H of the Ge-H bond that produced that vibration through a proportionality constant A (cm^{-2}) according to [25-29]

$$I \, (cm^{-1}) = \int [\alpha(\omega)/\omega] \, d\omega \; = \; (1/A) \cdot N_H \qquad (1)$$

where $\alpha(\omega)$ is the absorption coefficient and ω the vibration frequency, or wavenumber (cm^{-1}), of that mode. $\alpha(\omega)$ was determined by the Brodsky et al. formula for the transmittance [25].

The integral is calculated only in the absorption mode region of interest of the Ge-H peak under study. In this paper the density of the various Ge-H bonds is evaluated by using the peaks of the stretching mode range in an FTIR spectrum. The stretching mode range includes all the Ge-H bonds [25, 28, 29]. Hence the total density of H bonded to Ge, N_H^{total}, is obtained by summing up the H bond concentrations extracted from each peak of the stretching mode (SM) after applying eq. (1). The stretching mode often consists of two peaks so that

$$N_H^{total} = A_{1S} \cdot I_{1S} \; + A_{2S} \cdot I_{2S}$$

with I_{1S} and I_{2S} the integrated intensities of the stretching peak at low and high frequency, respectively, and A_{1S} and A_{2S} the associated proportionality constants. Some authors used only one value for A, either $5 \cdot 10^{19}$ cm^{-2} [30] or $6 \cdot 10^{19}$ cm^{-2} [31], for both stretching peaks. On the contrary, Arrais et al. [3] and Soukup et al. [32] assigned two different values to the A constants, namely $5 \cdot 10^{19}$ cm^{-2} and $1.4 \cdot 10^{20}$ cm^{-2} for the low and high frequency absorption peak, respectively. In the case of hydrogenated a-Si, based on a calibration of FTIR with NRA (Nuclear Reaction Analysis) [26] and ERDA [27] it was suggested that an average between the two different A_S can be tolerably used for the evaluation of the Si-H bonds by FTIR. Although, to the authors' knowledge, similar calibration has not been made for a-Ge:H, it is similarly assumed here that instead of two different A_S values for the low

and high frequency peaks an average between $5 \cdot 10^{19}$ cm^{-2} and $1.4 \cdot 10^{20}$ cm^{-2} can be used, i.e. $A_{av} = 9.5 \cdot 10^{19}$ cm^{-2}.

Secondary Neutral Mass Spectrometry (SNMS, type INA-X produced by SPECS GmbH, Berlin) was employed to measure the in-depth distribution of H within the samples [33, 34]. The surface bombardment and post ionization of sputtered neutral particles were performed at low pressure Electron Cyclotron Wave Resonance (ECWR) argon plasma. In the direct bombardment mode, Ar$^+$ ions are extracted from low pressure plasma and bombard a negatively biased (-350 V) sample surface with a current density of ~1mA/cm^2, performing a controlled surface erosion. The investigated area was confined within a circle of 2 mm diameter by a Ta mask. Post-ionized neutral particles are directed into a quadruple mass spectrometer Balzers QMA 410 by electrostatic lenses and a broad-pass energy analyzer. The lateral homogeneity of ion bombardment was checked by measuring the shape of the sputtered crater with an AMBIOS XP-1 type profilometer. A profilometer was also used to determine the sputtering rate by measuring both the crater depth and sputtering time.

The morphology of the sample surface was analysed by using a stylus profiler (Bruker, DEKTAK-XT). The use of a stylus profiler was dictated by the large extension (even up to some tens of micrometers) of the surface features in the annealed samples. The stylus tip was loaded with 12 mg weight and had a radius of 2.5 μm. The 3D images were recorded using a 400 μm scan length and 100x2 μm pitch. Data evaluation was done using the free software Gwyddion. A scanning electron microscope (SEM Hitachi S-4300 CFE) operated at 15 keV was also used for observation of the surface morphology of samples after annealing.

3 . Results and discussion

FTIR spectra of unannealed and annealed a-Ge:H/ZnSe deposited under a partial pressure of H=0.6 and H=0.9 (ERDA hydrogen content of 18 and 21 at%, respectively) are shown in figs. 2 a)-b). Gaussian deconvolution, not shown here, evidenced that the spectra consist of two peaks. For the sample with H=0.6 the spectrum is made up of two absorption bands at (1885±2) cm^{-1} and (1987±9) cm^{-1} while for the sample with H=0.9 the two

deconvoluted peaks are positioned at (1890 ± 5) cm^{-1} and (1991 ± 8) cm^{-1}. These values are in fairly good agreement with literature data that report on two absorptions at either 1880 or 1885 and 1980 cm^{-1} in the stretching mode range of a-Ge:H [30-32, 35-39]. The low-frequency vibration has to be ascribed to H bonded to a vacancy, i.e. to Ge with one dangling bond forming the GeH monohydride, while the high-frequency one is associated with the GeH$_2$ dihydride [30-32, 35-37, 39]. Fig. 2 shows that for both H pressures the stretching peak at low-frequency decreases while the one at high frequency increases by increasing the annealing time.

Such results can be quantified by using the integrated areas of each deconvoluted vibration, i.e. the value I of the integral in eq. (1), and their ratio. Since in the following we will compare the evolution of the H bonding configuration as a function of annealing time and H concentration, it is not necessary to know the absolute concentration N_H of each bond state of the H to Ge as N_H is proportional to the related I apart from a constant. In particular, the comparison is carried out by employing the so called microstructure parameter R [29, 35, 40, 41] defined as R= [GeH$_2$] / ([GeH] + [GeH$_2$]) = $I_{S2}/(I_{S1} + I_{S2})$ where the square brackets [ ] indicate concentrations while I_{S1} and I_{S2} are the integrated intensities of the FTIR vibrational modes of GeH and GeH$_2$, respectively. When R is low the hydrogen is mainly incorporated under the monohydride groups.

Fig. 3 displays the plots of the microstructure parameter R as a function of the H partial pressure, i.e. H concentration, for the different annealing times. The behavior of R shows that the GeH$_2$ groups are always present in the samples with partial pressure of H=0.6 and H=0.9 whichever is the annealing time. Their density increases with increasing annealing time for a given H concentration (Fig. 3). For H=0.2 the existence of the polyhydrides (GeH$_2$) is detected only at the annealing time of 120 min. As reported in the literature [35-37, 42, 43] the polyhidrides reside on the surfaces of microvoids where Ge atoms with two or more open dangling bonds are likely to exist. The mentioned microvoids are reported to typically exist in any amorphous material [36, 38, 44-47]. Nanovoids in a-Ge as small as 0.5 nm that can host 10-20 free dangling bonds on each void surface have been reported [38].

Thermal annealing also influences the morphology of the samples as evidenced by the formation of surface blisters. They are not detected in the unannealed samples and in

not-hydrogenated films regardless of any applied annealing. Fig. 4 a) is a typical stylus profiler image of such blisters. Their average lateral size increases with increasing H concentration (Fig. 5). However, the size decreases for H = 0.9 with respect to the lower H concentrations (Fig. 5). This is due to the formation of craters when H=0.9 (Fig. 4 b). The latter ones are as deep as the whole Ge deposit and have an average size of 28.2 μm which is right the maximum size of the blisters in samples with H=0.6 annealed for 120 min. This supports the hypothesis that the craters are blown blisters and that blisters greater than ˜28 μm are unstable and explode. The blisters visible in the H=0.9 sample are those which were not enough big for blowing. The bursting of the biggest blisters explains the low value of the average blister diameter (16.2 μm) measured in the sample with H=0.9. The result that the average size of the blisters in the sample with H=0.9 is only 16.2 μm (annealing for 120 min) (Fig. 5) suggests that the size threshold for blowing is smaller when the H concentration is high. The average blister height exhibits exactly the same trend as the diameter reaching a maximum of 0.96 μm for the H=0.6 sample annealed for 120 min while the minimum value is 0.17 μm measured in the H=0.9 sample treated for 40 min.

The evolution of the Ge-H bonding configuration and the behaviour of the blister size upon annealing seem to suggest that they are related to each other.

The SM vibration at low wavenumber of 1885÷1890 cm^{-1} has to be ascribed to the presence of monohydride (GeH) bonds, as recalled earlier. The monohydrides are dispersed isolated network sites and are associated with H bonded at isolated dangling bonds and vacancies [35, 42, 43]. The FTIR peak at the higher wavenumber of 1987÷1991 cm^{-1} is instead associated with polymers, like GeH_2 dihydrides and polygermane chains $(GeH_2)_n$, $n\geq2$, on the internal surfaces of voids [31, 35, 42, 48]. Very likely also clusters of monohydrides, i.e. $(GeH)_n$ groups, can contribute to the second peak at high frequeny of the stretching range as reported for a-Si:H [25-28, 40, 44]. The increase of the microstructure parameter R, i.e., of the density of the GeH_2 groups and related polygermanes $(GeH_2)_n$, $n\geq2$, in the annealed samples (Fig. 3) can be due to the thermal activation of H atoms that have occupied interstitial sites, i.e. shallow traps, during sputtering. Their binding energy is expected to be quite low similarly to what observed in a-Si where it is around 0.2-0.5 eV [45]. Very likely such H atoms, upon annealing, may locally rearrange their positions by

breaking weak Ge-Ge bonds and forming additional Ge-H bonds. The latter ones could be of the dihydride type, GeH_2, when the rearrangement involves near-neighbouring H atoms.

The expected increased diffusivity of H interstitials associated with the anneal temperature can further favour their search for free Ge dangling bonds to which they can bond. It should be noted that the decrease of the strength of the low frequency SM band implies that the density of the isolated monohydrides has decreased suggesting a partial decomposition of the GeH groups. However, the GeH groups could also have undergone clustering forming $(GeH)_n$, $n>1$, clusters. As said earlier, the latter ones vibrate at the same frequency as the GeH_2 bonds so that it is not possible to establish their contribution to the microstructure parameter R and how far the GeH decomposition is effective. Differently from the monohydrides, the GeH_2 groups and related chains $(GeH_2)_n$ most often prefer to reside on the surfaces of (micro)voids [31, 35, 42, 48]. The great increase of the concentration of the GeH_2 dihydrides upon annealing supports the hypothesis that nano-voids present in the as-deposited state have become quite larger in size as they have to accommodate a higher number of the GeH_2 dihydrides on their surfaces. As reported above, the size of the surface blisters also increases with increasing annealing time (Fig. 5) which suggests that the blisters have likely originated from the voids whose walls are decorated by the dihydrides. One more mechanism for the increase of the void size from the nanometer to the micrometer scale could have been by the coalescence of near-neighbouring voids.

The formation of craters as big as the largest blisters in the a-Ge films with the H partial pressure of H=0.9 submitted to the longest (120 min) heat treatment suggests that the craters are blisters that have undergone bursting because of a too high internal pressure. The blisters are thus cavities containing a gas. It is proposed that the gas is molecular H_2.

The hypothesis of the presence of H_2 gas in the voids is supported by three experimental evidences. The first one is the activation energy E_a for the onset of blister formation measured by Arrhenius plots reporting the minimum time t needed to make the blisters optically visible as a function of the temperature T [49]. The temperature range investigated was 179-206 °C. Such temperatures higher than the one of annealing (135 °C) were chosen to reduce the onset time. To measure it hydrogenated samples have been heated on a plate at constant temperature (± 1 °C) while illuminated by a He-Ne laser beam with diameter of 3 mm and angle of incidence of 60° which resulted in about 3x6 mm elliptically illuminated

sample area. After reflection the radiation falls into a Si PIN detector with diameter of 8 mm. During the annealing process the specular reflection transforms into a spread one, which has a dominant directional component that is partially diffused by surface irregularities. The onset of blistering was identified with the decreasing of the reflected intensity caused by the outgoing rays reflected at many different angles. The sampling rate of the reflection monitoring was 10 sec. Fig. 6 is the image of blisters soon after they had shown up. The t vs 1/T data are reported in the Arrhenius plot of Fig. 7 for the sample with H partial pressure H=0.9. The activation energy E_a is derived from Fig. 7 using the Arrhenius relationship

$$1/t = A \cdot \exp (-E_a/kT)$$

with t the blistering onset time, A a constant, k the Boltzman constant and T the absolute temperature. It turns out to be E_a = 1.65 eV (estimated error ± 10%).

Activation energies determined as done in this work have been identified as the binding energies of the SiSi and GeGe bonds, respectively, in Si and Ge hydrogenated by H implantation leading to the conclusion that the rupture of those host lattice bonds is the initial key step for the generation of the blisters [49]. We believe that the bond of the host atom to H, i.e. Ge-H bond in our case, has to be taken into account rather than the GeGe one because the breakage of the latter does not make available any free H, which is instead necessary to make any nanocavity to start to grow. On the contrary, the break of the GeGe bonds, when annealing is applied, produces new Ge dangling bonds where H atoms can attach to instead of remaining free. Moreover, the GeGe enthalpy in a-Ge is much greater than the measured E_a as it varies in the range 2.68-2.81 eV [3, 38].

The bond energy of GeH lies in the range 2.99-3.33 eV [3, 38, 50] with an average value among the three cited references of 3.16 eV. The break of only one GeH bond does not account for the observed E_a. However, the break of two GeH bonds with simultaneous formation of a hydrogen molecule implies a change of energy $\Delta \varepsilon = 2 \cdot \varepsilon (GeH) - \varepsilon (H_2) =$ 1.82 eV, with $\varepsilon (GeH)$ the bonding energy of GeH (3.16 eV) and $\varepsilon (H_2)$ = 4.5 eV the one of the H_2 molecule [51, 52]. The 1.82 eV value reasonably well agrees with the experimental activation energy E_a=1.65 eV for the blistering onset. Such agreement would

suggest that the mechanism for blister formation and growth implies the simultaneous rupture of two GeH bonds and creation of the H_2 molecule. The measured E_a for blistering onset is thus an effective activation energy resulting from the energy balance between these two events. Following the suggestion by Weldon et al. [11] and Bedell et al. [53] the lower E_a value with respect to the expected one could be ascribed to the fact that the thermal energy supplied by annealing also serves to enhance the pressure in the nanovoids. The size increase of the latter ones is thus not merely due to the breakage of the GeH bonds (as assumed in the Arrhenius theory) but also to the increased inside pressure. This ''pressure-induced activation'' *de facto* reduces the value of the temperature at which the blisters start to appear on the surface [11]. It should, however, be noticed that the partial disagreement between measured and estimated activation energies can also be ascribed to the scatter of the literature data for the bonding energy of GeH, ε (GeH).

The second experimental evidence is supplied by the behaviour of the total concentration of the Ge-H bonds. For what said earlier, the latter one is proportional to the total integrated area of the stretching mode range, I_{SM}^{Total}, obtained by summing up the integrated intensities of the two deconvoluted SM peaks at low and high frequency. I_{SM}^{Total} is plotted in Fig. 8 as a function of the H partial pressure and anneal time. As expected, I_{SM}^{Total}, i.e. the total concentration of the Ge-H bonds, increases with increasing H partial pressure. However, for each H partial pressure it decreases with respect to the unannealed case by increasing the anneal time. This indicates that the density of the H atoms bonded to Ge has decreased, i.e. that a certain amount of Ge-H bonds have broken with release of atomic H. The thermal energy supplied by the annealing treatment is the driven force for the rupture of the Ge-H bonds.

For the GeH_2 polymers residing on the walls of voids the H atoms are liberated into the voids themselves where they may react to form molecular H_2. For isolated Ge-H bonds the released H atoms may undergo either one of two processes. Either they gather into platelets wherefrom nascent nanovoids can nucleate and grow in size or they occupy interstitial sites from which they can move toward nearby voids by thermally activated diffusion and contribute to the formation of additional molecular H_2. By the gas law, upon annealing the molecular H_2 inside the voids expands which results in an increase of the volume of the voids. The larger inner surfaces associated with such large cavities offer additional Ge sites

with two or more open dangling bonds where formation of additional GeH_2 polymers is likely to take place. The H atoms release and reaction to produce more H_2 can thus continue.

The surface blisters are produced when the voids reach such a big size to cause deformation of the layer surface. The blisters thus correspond to bubbles containing molecular H_2. They have developed from GeH_2 decorated nano- and micron-sized cavities which have increased their volume because of the increase of the inside pressure due to the thermal expansion of the H_2 gas upon annealing. Eventually, the H_2 filled cavities will lift off to such an extent to give rise to observable blisters and then craters. The latter ones supply the way for the escape of the unbound hydrogen from the samples.

Both ERDA (Fig. 1) and SNMS (Fig. 9) supply the third experimental evidence in support of the above described processes. ERDA (Fig. 1) shows that the total H content is lower in the annealed samples with respect to the not-annealed ones for the highest H partial pressures of H=0.9 and also H=0.6 (only for 120 min anneal), i.e. in samples exhibiting craters. The most likely explanation for this behaviour is that H has left the related annealed samples.

SNMS was employed to confirm this interpretation. In order to better evidence the effect of annealing on the in-depth spatial distribution of H, annealing times shorter than those discussed so far were also applied, namely 10 min. Fig. 9 shows the typical SNMS profile of H in a sample exhibiting craters (H=0.9, annealing time 40 min) compared with the H profile in a sample for which craters were not detected (H=0.9, annealing time 10 min). At the bottom of the a-Ge layer (depth ˜500 nm) the hydrogen concentration measured by SNMS is the same as the ERDA one (21%) for both samples. In the 10 min annealed sample it stays nearly constant for the first about 200 nm above the interface to the substrate and then decreases very slowly to about 15% in the top part of the layer. On the other hand, in the sample annealed for 40 min the H continuously decreases very fast starting from the interface to the substrate being totally absent in the top 10 nm of the layer (■: blue curve). Hydrogen depletion as a consequence of annealing time is pretty evident. The H depletion gradient increases with increasing annealing temperature. In the annealed films with surface craters the most efficient route for the escape out of H is by far by the opening of the observed craters. Escape can also take place through a network of

interconnected nano and microvoids with some branch emerging at the surface. The loss of H is expected to have similarly occurred by the latter mechanism in the craters-free annealed samples, i.e. annealed for short times and/or with low H concentration. For such type of samples the SNMS result, i.e. depletion of H only in the top part of the a-Ge layer (●: black H profile in Fig. 9), could be ascribed to the insufficient time for H_2 to diffuse to the top surface from deeper distances. It might also be that the effective pathway of interconnected voids is made only of small voids close to the top surface because they had no sufficient time to enlarge enough to establish many connections among each other, especially to voids deeper and deeper in the a-Ge film.

4 . Conclusions

The origin of surface blisters and craters in annealed RF sputtered a-Ge:H films has been investigated by several techniques (FTIR, ERDA, SNMS, stylus profilometry and Arrhenius plots). In the as-deposited, unannealed films H is incorporated as GeH monohydrides and no blister formation is observed. Instead, annealing favours the formation of GeH_2 dihydrides that decorate the inner surfaces of voids. The increase of their density makes the void size to increase. The thermal treatment also causes the rupture of the Ge-H bonds, especially the GeH_2 dihydride ones, with consequent release within the voids of atomic H that reacts to form molecular H_2. The thermal expansion of the H_2 gas additionally contributes to increase the volume of the voids to such an extent to lift up the film surface giving rise to randomly distributed blisters. Because of the presence of such blisters faulted performance of a-Ge:H based devices submitted to annealing in whatever step of the manufacturing process has to be expected. In fact, irregular interfaces among the layers constituting the device as well as possible short circuit channels in the case of craters, if present, can occur. Moreover, the mentioned rupture of Ge-H bonds leads to the creation of free dangling bonds, previously passivated by H, that act as non-radiative recombination centers for the minority carriers.

Acknowledgements

References

[1] Volker Steenhoff, Alex Neumüller, Oleg Sergeev, Martin Vehse, Carsten Agert, *Sol. Energy Mater. Sol. Cells* 2016, **95**, 148-153.

[2] M. Moreno, N. Delgadillo, A. Torres, R. Ambrosio, P. Rosales, A. Kosarev, C. Reyes-Betanzo, J. de la Hidalga-Wade, C. Zuniga, W. Calleja, *Appl. Surf. Sci.* 2013, **267**, 533-538

[3] A. Arrais, P. Benzi, E. Bettizzo and C. Damaria, *J. Phys. D: Appl. Phys.* 2009, **42**, 105406.

[4] D. L. Staebler, C. R. Wronski, *Appl. Phys. Lett.* 1977, **31**, 292–294.

[5] M. J. M. Pathak, K. Girotra, S. J. Harrison, J. M. Pearce, *Sol. Energy* 2012, **86**, 2673–2677.

[6] M. J. M. Pathak, J. M. Pearce, S. J. Harrison, *Sol. Energy Mater. Sol. Cells* 2012, **100**, 199–203

[7] J. Whitaker, M. M. de Lima, F. C. Marques, P. C. Taylor, *J. Non-Cryst. Solids* 2004, **338-340**, 374-377

[8] T. Aoki, H. Shimada, W. Q. Sheng, K. Shimakava, *Phil. Mag. Lett.* 1997, **75**, 163-167

[9] Bernard Terreault, *Phys. Stat. Sol.* (a) 2007, **204**, 2129–2184

[10] S. Reboh, F. Schaurich, A. Declemy, J. F. Barbot, M. F. Beaufort, N. Cherkashin, and P. F. P. Fichtner, *J. Appl. Phys.* 2010, **108**, 023502

[11] M. K. Weldon, V. E. Marsico, Y. J. Chabal, A. Agarwal, D. J. Eaglesham, J. Sapjeda, W. L. Brown, D. C. Jacobson, Y. Caudano, S. B. Christman, and E. E. Chaban, J. *Vac. Sci. Technol. B* 1997, **15**, 1065-1073

[12] Fan Yang, Xuan Xiong Zhang, Tian Chun Ye, and Song Lin Zhuang, *J. Electrochem. Soc.* 2011, **158**, H1233-H1237

[13] A. S. Kuznetsov, M. A. Gleeson, and F. Bijkerk, *J. Appl. Phys.* 2013, **114**, 113507

[14] C. Roch and J. C. Delgado, *Thin Solid Films* 1992, **221**, 17-20

[15] R. Rüther, J. Livingstone, *Thin Solid Films* 1994, **251**, 30-35

[16] A. H. Mahan, B. Roy, R. C. Reedy, Jr., D. W. Readey, and D. S. Ginley, *J. Appl. Phys.* 2006, **99**, 023507

[17] C. Frigeri, M. Serényi, A. Csik, Zs. Szekrényes, K. Kamarás, N. Q. Khánh, L. Nasi, *Appl. Surf. Sci.* 2013, **269**, 12-16

[18] M. Serényi, C. Frigeri, Zs. Szekrényes, K. Kamarás, L. Nasi, A. Csik, N. Q. Khánh, *Nanoscale Research Letters* 2013, **8**, 84

[19] C. Frigeri, M. Serényi, Zs. Szekrényes, K. Kamarás, A. Csik, N. Q. Khánh, *Sol. Energy* 2015, **119,** 225-232

[20] C. Frigeri, M. Serényi, N. Q. Khánh, A. Csik, L. Nasi, Z. Erdélyi, D. L. Beke and H.-G. Boyen, *Appl. Surf. Sci.* 2013, **267**, 30-34

[21] L. de los Santos Valladares, A. Bustamante Dominguez, J. Llandro, S. Holmes, O. Avalos Quispe, R. Langford, J. Albino Aguiar, C. H. W. Barnes, *Appl. Surf. Sci.* 2014, **316,** 15-21

[22] N. Q. Khánh, M. Serényi, A. Csik, C. Frigeri, *Vacuum* 2012, **86,** 711-713.

[23] E. Kótai, *Nucl. Instrum. Methods Phys. Res. B* 1994, **85,** 588-596.

[24] Z. Zolnai, M. Toporkov, J. Volk, D.O. Demchenko, S. Okur, Z. Szabó, Ü. Özgür, H. Morkoç, V. Avrutin, E. Kótai, *Appl. Surf. Sci.* 2015, **327,** 43-50.

[25] M. H. Brodsky, M. Cardona, and J. J. Cuomo*, Phys. Rev. B* 1977, **16,** 3556-3571.

[26] A. A. Langford, M. L. Fleet, B. P. Nelson, W. A. Lanford, N. Maley, *Phys. Rev. B* 1992, **45**, 13367-13377.

[27] G. Amato, G. Della Mea, F. Fizzotti, C. Manfredotti, R. Marchisio, A. Paccagnella, *Phys. Rev. B* 1991, **43,** 6627-6632.

[28] C. Manfredotti, F. Fizzotti, M. Pastorino, P. Polesello, E. Vittone, *Phys. Rev. B* 1994, **50,** 18046-18053.

[29] J. Daey Ouwens and R. E. Schropp, *Phys. Rev. B* 1996, **54,** 17759-17762

[30] A. Kosarev, A. Torres, Y. Hernandez, R. Ambrosio, C. Zuniga, T. E. Felter, R. Asomoza, Y. Kudriavtsev, R. Silva-Gonzalez, E. Gomez-Barojas, A. Ilinski, A. S. Abramov, *J. Mater. Res*. 2006, **21,** 88-104

[31] Y. Bouizem, A. Belfedal, J. D. Sib, A. Kebab, L. Chahed, *J. Phys. Condens. Matter* 2007, **19,** 356215.

[32] R. J. Soukup, N. J. Ianno, S. A. Darveau, C. L. Exstrom, *Sol. Energy Mater. Sol. Cells* 2005, **87,** 87–98

[33] H. Oechsner, *Nucl. Instrum. Methods Phys. Res B* 1988, **33,** 918-925.

[34] K. Vad, A. Csik, G. A. Langer, *Spectroscopy Europe* 2009, **21,** 13-17.

[35] M. Mulato, I. Chambouleyron, I. L. Torriani, *J. Appl. Phys.* 1996, **79**, 4453-4455.

[36] R. A. Rudder, J. W. Cook Jr., G. Lucovsky, *Appl. Phys. Lett*. 1984, **45**, 887–889.

[37] B. A. Nadzhafov, G. I. Isakov, *J. Appl. Spectrosc.* 2005, **72**, 396-402.

[38] G. A. N. Connell and J. R. Pawlik, *Phys. Rev. B* 1976, **13,** 787-804

[39] D. Bermejo and M. Cardona, *J. Non-Cryst. Solids* 1979, **32,** 421-430.

[40] M. Daouahi, K. Zellama, H. Bouchriha**,** P. Elkaïm, *Eur. Phys.-J. Appl. Phys.* 2000, **10**, 185-191

[41] A. H. Mahan, P. Raboisson, R. Tsu, *Appl. Phys. Lett.* 1987, **50,** 335–337.

[42] G. Lucovsky, S. S. Chao, J. Yang, J. E. Tyler, R. C. Ross and W. Czubatyj, *Phys. Rev. B* 1985, **31**, 2190-2197.

[43] K. W. Jobson, J.-P. R. Wells, R. E. I. Schropp, D. A. Carder, P. J. Philips, J. I. Dijkhuis, *Phys. Rev. B* 2006, **73,** 155202.

[44] H. Touir, K. Zellama, J.-F. Morhange, *Phys. Rev. B* 1999, **59,** 10076-10083.

[45] S. Acco, D. L. Williamson, P. A. Stolk, F. W. Saris, M. J. van den Boogaard, C. Sinke, W. F. van der Weg, S. Roorda, P. C. Zalm, *Phys. Rev. B* 1996, **53,** 4415-4427.

[46] A. H. Mahan, Y. Xu, D. L. Williamson, W. Beyer, J. D. Perkins, M. Vanecek, L. M. Gedvilas, B. P. Nelson, *J. Appl. Phys*. 2001, **90,** 5038-5047.

[47] Hung-Ju Lin, Sheng-Hui Che, *Opt. Mater. Express*. 2013, **3,** 1215-1222.

[48] D. Comedi, F. Dondeo, I. Chambouleyron, Z. L. Peng, and P. Masher, *J. Non-Cryst. Solids* 2000, **266–269,** 713-716.

[49] Q.-Y. Tong, K. Gutjahr, S. Hopfe, U. Gösele, T.-H. Lee, *Appl. Phys. Lett.* 1997, **70**, 1390-1392

[50] R. Tsu, D. Martin, J. Gonzales-Hernandez, and S. R. Ovshinsky, *Phys. Rev. B* 1987, **35,** 2385-2390

[51] P. Gupta, V. L. Colvin, and S. M. George, *Phys. Rev. B* 1988, **37,** 8234-8243.

[52] W. Beyer, *Physica B* 1991, **170,** 105-114.

[53] S. W. Bedell and W. A. Lanford, *J. Appl. Phys*. 2001, **90,** 1138-1146

Figure Captions

Figure 1. Hydrogen content in the as-deposited, not annealed films (● symbol) as determined by ERDA as a function of the H partial pressure P_H (expressed in units of % of the 2.5_x10^{-2} mbar plasma pressure). The plot also shows the hydrogen ERDA concentrations for the annealed samples to be discussed later in the paper. ■: annealed for 40 min, ▲: annealed for 120 min.

Figure 2. a) Typical IR absorption spectra in the stretching mode range of the wavenumber for the sample with H partial pressure of 0.6 for no anneal (black spectrum A), anneal times of 40 min (red spectrum B) and 120 min (blue spectrum C). b) As a) for the sample with H partial pressure of 0.9.

Figure 3. Plot of the microstructure parameter R as a function of the H partial pressure P_H (expressed in units of % of the 2.5_x10^{-2} mbar plasma pressure) for the different annealing times. Dash-dot line for t=0 min (no anneal), dashed line for t=40 min, solid line for t=120 min.

Figure 4. Stylus profilometer morphological images of the samples annealed for 120 min deposited with a) H partial pressure 0.6 and b) H partial pressure 0.9. The black areas in b) are craters as deep as the a-Ge layer (530 nm).

Figure 5. Average blister diameter <D> as a function of the H partial pressure P_H (expressed in units of % of the 2.5_x10^{-2} mbar plasma pressure) for the different annealing times. Dashed line for t=120 min, solid line for t=40 min.

Figure 6. a) SEM image of blisters taken soon after their formation. b) SEM intensity (height) profile across the yellow arrowed blister, from left to right.

Figure 7. Arrhenius plot of the *ln* of the inverse minimum time t for optical detection of the surface blisters as a function of the inverse of the absolute anneal temperature. Sample with H partial pressure H=0.9.

Figure 8. Total integrated area of the stretching mode range, I_{SM}^{Total}, as a function of the H partial pressure P_H (expressed in units of % of the 2.5_x10^{-2} mbar plasma pressure) for the different annealing times. Dash-dot line for t=0 min (no anneal), dashed line for t=40 min, solid line for t=120 min.

Figure 9. SNMS plot of the in-depth H concentration as a function of the film thickness in a sample hydrogenated with a partial pressure of H=0.9 submitted to annealing at 135 °C for 10 min (●: black curve) and 40 min (■: blue curve). The sudden decrease of the concentration displayed by the black curve in the very top layers is due to a 5-10 nm thick oxidized layer.
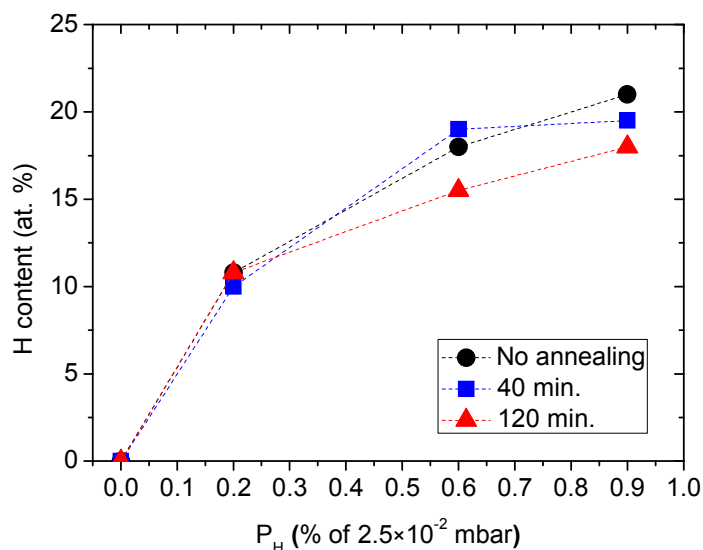
Figure 1. Hydrogen content in the as-deposited, not annealed films (● symbol) as determined by ERDA as a function of the H partial pressure P_H (expressed in units of % of the 2.5_x10^{-2} mbar plasma pressure). The plot also shows the hydrogen ERDA concentrations for the annealed samples to be discussed later in the paper. ■: annealed for 40 min, ▲: annealed for 120 min.
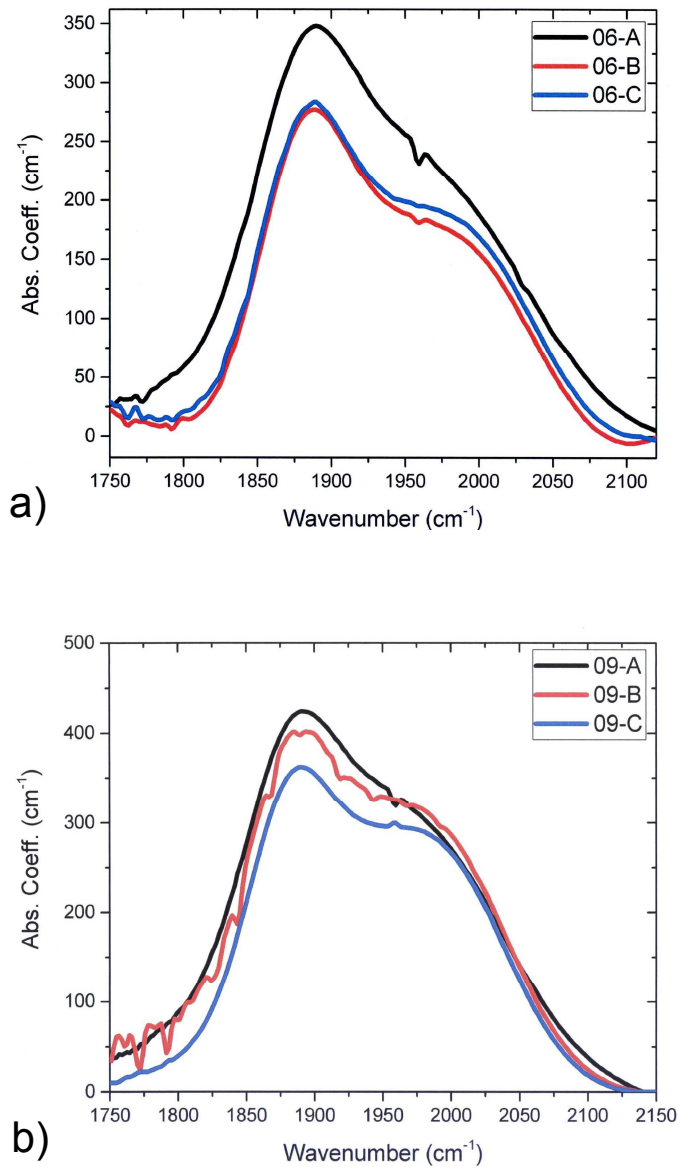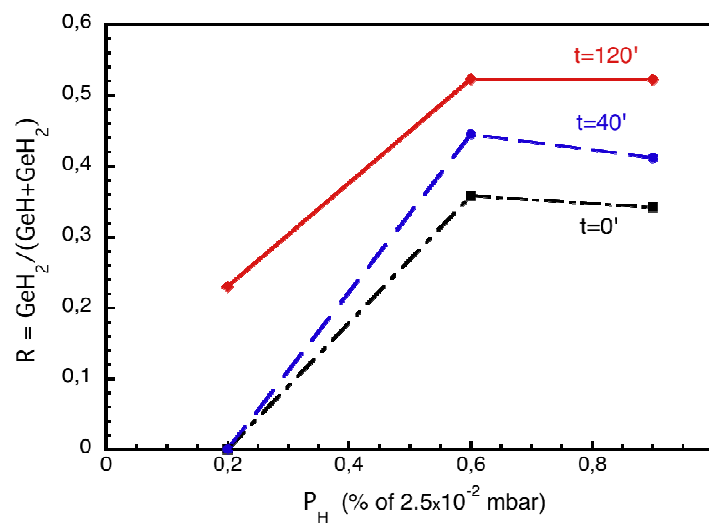
Figure 2. a) Typical IR absorption spectra in the stretching mode range of the wavenumber for the sample with H partial pressure of 0.6 for no anneal (black spectrum A), anneal times of 40 min (red spectrum B) and 120 min (blue spectrum C). b) As a) for the sample with H partial pressure of 0.9.

Figure 3. Plot of the microstructure parameter R as a function of the H partial pressure P_H (expressed in units of % of the 2.5_x10^{-2} mbar plasma pressure) 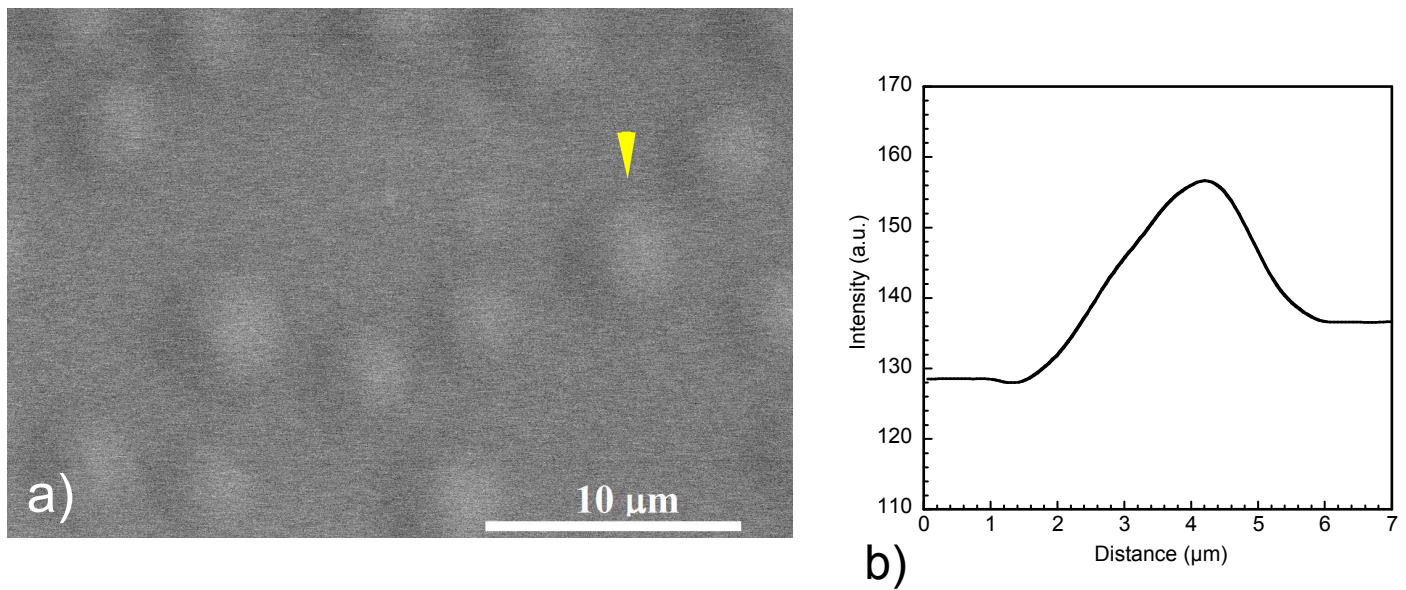for the different annealing times. Dash-dot line for t=0 min (no anneal), dashed line for t=40 min, solid line for t=120 min.

Figure 4. Stylus profilometer morphological images of the samples annealed for 120 min deposited with a) H partial pressure 0.6 and b) H partial pressure 0.9. The black areas in b) are craters as deep as the a-Ge layer (530 nm).

Figure 5. Average blister diameter <D> as a function of the H partial pressure P_H (expressed in units of % of the 2.5_x10^{-2} mbar plasma pressure) for the different annealing times. Dashed line for t=120 min, solid line for t=40 min.

Figure 6. a) SEM image of blisters taken soon after their formation. b) SEM intensity (height) profile across the yellow arrowed blister, from left to right.
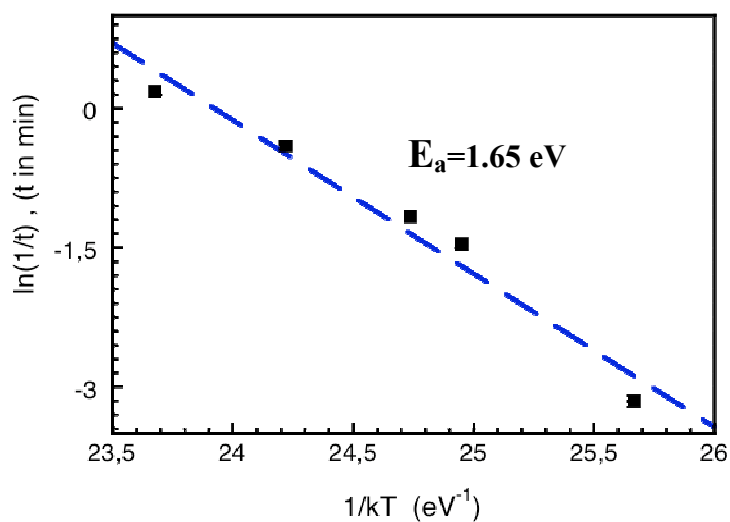
Figure 7. Arrhenius plot of the *ln* of the inverse minimum time t for optical detection of the surface blisters as a function of the inverse of the absolute temperature. Sample with partial pressure H=0.9.
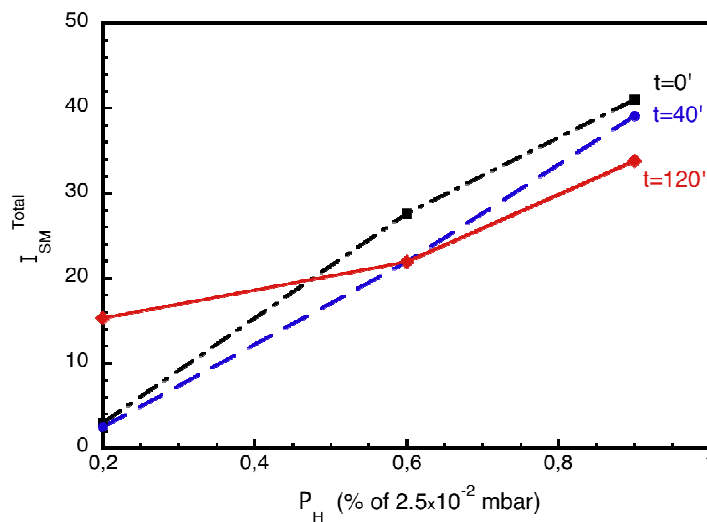
Figure 8. Total integrated area of the stretching mode range, I_{SM}^{Total}, as a function of the H partial pressure P_H (expressed in units of % of the 2.5×10^{-2} mbar plasma pressure) for the different annealing times. Dash-dot line for t=0 min (no anneal), dashed line for t=40 min, solid line for t=120 min.
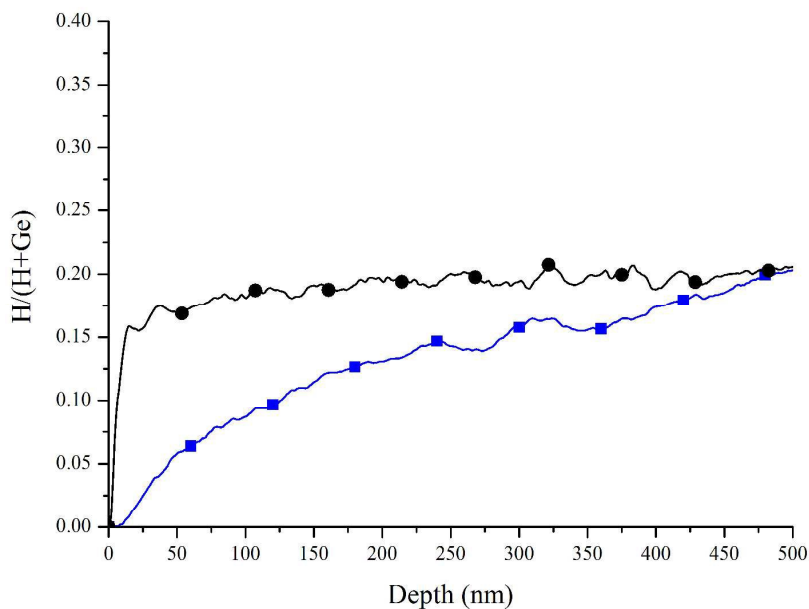
27

Figure 9. SNMS plot of the in-depth H concentration as a function of the film thickness in a sample hydrogenated with a partial pressure of H=0.9 submitted to annealing at 135 °C for 10 min (●: black curve) and 40 min (■: blue curve). The sudden decrease of the concentration displayed by the black curve in the very top layers is due to a 5-10 nm thick oxidized layer.